Transverse spin freezing in a-$(Fe_{1-x}Mn_x)_{78}Si_8B_{14}$: A site-frustrated metallic glass

D. H. Ryan, A. D. Beath, and E. McCalla
Physics Department and Centre for the Physics of Materials, McGill University, 3600 University Street, Montreal, Quebec, Canada H3A 2T8

J. van Lierop
Materials Science Department, Brookhaven National Laboratory, Upton, New York 11973

J. M. Cadogan
School of Physics, The University of New South Wales, Sydney, NSW 2052, Australia
(Received 5 August 2002; published 14 March 2003)

Muon spin relaxation, Mössbauer spectroscopy, magnetization, and ac-susceptibility have been used to investigate transverse spin freezing in a site-frustrated alloy system. All static and dynamic signatures coincide to yield a well-defined transition temperature (T_{xy}). These results are in full agreement with numerical simulations and earlier work on bond-frustrated alloys. No evidence is found for a third transition below T_c and T_{xy}. A complete magnetic phase diagram for a-$(Fe_{1-x}Mn_x)_{78}Si_8B_{14}$ is presented.

DOI: 10.1103/PhysRevB.67.104404 PACS number(s): 75.50.Lk, 76.75.+i, 76.80.+y, 75.50.Kj

I. INTRODUCTION

The random addition of antiferromagnetic (AF) exchange interactions to an otherwise ferromagnetic (FM) Heisenberg spin system leads to a loss of FM order through the effects of exchange frustration. In extreme cases, a spin glass (SG) is formed with random isotropic spin freezing and neither net magnetization nor long range order. At lower levels of frustration the system exhibits characteristics of both extremes, as long-ranged FM order coexists with SG order in the plane perpendicular to the FM order.[1] On warming such a system from $T=0$ K, the SG order first melts at T_{xy} followed by the loss of FM order at T_c. This picture has emerged from experimental measurements,[2] numerical simulations,[3] and mean-field calculations.[4] The infinite-ranged interactions implicit in mean-field spin glass models make all forms of exchange frustration equivalent. However, real systems are generally dominated by shorter-ranged interactions, and for the case of first-neighbor-only exchange coupling two distinct situations can be identified: (i) bond frustration[3] and (ii) site frustration.[5]

Bond frustration arises when each exchange bond to a moment's nearest neighbors may be either positive (i.e., ferromagnetic) or negative (i.e., antiferromagnetic). Perhaps the best experimental example of this case is provided by iron-rich a-Fe_xZr_{100-x}.[2,6] Here the competing exchange interactions arise from the distance dependence of the direct Fe-Fe exchange coupling combined with the distribution of nearest-neighbor distances inherent to the glass structure. Zero-field muon spin relaxation (ZF-μSR) has been used to establish the magnetic phase diagrams of two bond frustrated systems in great detail,[7,8] and has shown that the static and dynamic signatures of both T_c and T_{xy} coincide within experimental error: the fluctuation rate diverges at the same temperature at which static order develops. These results are in perfect agreement with the predictions of numerical simulations,[3] and a cross-check using selective excitation double Mössbauer spectroscopy has confirmed that the fluctuations sampled by interstitial muons and those seen at the nuclei of the moment-carrying iron atoms are identical.[9]

Site frustration is achieved by introducing a dopant with AF coupling to all of its nearest neighbors, so that the frustration is introduced sitewise rather than bondwise. While the gross magnetic behavior is expected to be the same as the bond frustrated case (the system exhibits noncollinear order at low temperatures, there are two magnetic transitions at intermediate dopings and a spin glass at higher dopings), numerical simulations show that there are two striking differences.[5] First, low levels of doping do not cause frustration. Isolated AF-coupled sites simply order antiparallel to the majority FM order, reducing the total magnetization, but not causing any noncollinearity. Frustration only appears when the dopant density is high enough for AF-AF pairs to occur. Second, the transverse correlations below T_{xy} exhibit short-range AF character rather than forming the xy spin glass observed in the bond frustrated case. The first of these distinctions has been verified experimentally in manganese-doped metallic glasses of the form a-(Fe,Mn)-G, where G is a mixture of two or more glass-forming metalloids that make up about 20 at.% of the material. The strong similarities in the phase diagrams of a-$(Fe_{1-x}Mn_x)_{75}P_{16}B_6Al_3$,[10–14] a-$(Fe_{1-x}Mn_x)_{75}P_{15}C_{10}$,[15] a-$(Fe_{1-x}Mn_x)_{77}Si_{10}B_{13}$,[16] and a-$(Fe_{1-x}Mn_x)_{78}Sn_2Si_6B_{14}$ (Ref. 17) serve to emphasize that it is the frustration introduced by the Mn that dominates the magnetic response and that the properties of the glass-former mix are largely unimportant. In all cases, the second transition does not appear until x reaches ~ 0.2. More significantly, Mössbauer spectroscopy in a-$(Fe_{1-x}Mn_x)_{78}Sn2Si_6B_{14}$,[17] and polarized neutron diffraction from a single crystal of Fe_2MnSi,[18] showed that the transverse spin components that order at T_{xy} do so orthogonally to the FM order established at T_c, and that they exhibit AF correlations, in full agreement with the numerical simulations.[5,19]

While the consistency between experiment and simulation for the two types of frustration appears excellent, one sharply conflicting result exists. A recent ZF-μSR study of

a-$(Fe_{0.74}Mn_{0.26})_{75}P_{16}B_6Al_3$ (Ref. 20) suggested that the static and dynamic signatures of transverse spin freezing at T_{xy} *did not* coincide. Drawing on additional data from Mössbauer spectroscopy,[21] small-angle neutron scattering,[22] inelastic neutron scattering,[23] and neutron depolarization,[24] Mirebeau *et al.* argued that their data provided evidence of *two* distinct transitions below T_c: a canting transition at T_K that leads to the development of noncollinearity but involves no dynamical anomaly, followed by a freezing transition at T_F which is associated with strong energy losses and a peak in the fluctuation rate, but no specific change in the magnetic correlations.

This three-transition interpretation of the magnetic ordering in this single sample is inconsistent with numerical simulations of site frustrated Heisenberg spin systems,[5,19] and the reported disagreement between the static and dynamic signatures of transverse spin freezing in the ZF-μSR data stands in stark contrast to the almost perfect agreement observed at T_{xy} in bond frustrated systems.[7,8,25,26] We have therefore revisited the system in order to clarify the situation. Here we report an extensive study of the entire magnetic phase diagram of a-$(Fe_{1-x}Mn_x)_{78}Si_8B_{14}$ for $0 \leqslant x \leqslant 0.5$, covering the full range of magnetic behavior from ferromagnetic to spin glass, with *five* compositions in the two-transition region. These materials have been studied using both bulk techniques (magnetization and susceptibility) and microscopic probes (Mössbauer spectroscopy and ZF-μSR). We find perfect agreement between the static and dynamic signatures of T_{xy} obtained from all techniques. There is no evidence of separate static and dynamic transitions below T_c. The phase diagram derived from our measurements is fully consistent with numerical simulations and the observed signatures of T_{xy} in this site frustrated material are identical to those observed previously in bond frustrated alloys.

II. EXPERIMENTAL METHODS

Ingots of $(Fe_{1-x}Mn_x)_{78}Si_8B_{14}$ were prepared by arc melting appropriate amounts of the pure elements (Fe 99.97%, Mn 99.99%, Si 99.9999% and B 99.5%) under Ti-gettered argon. These were then melt spun in 40-kPa helium using a wheel speed of 55 m/s to obtain the metallic glass samples. For $x \leqslant 0.20$, meter-length ribbons $\sim$1 mm wide were obtained, however as the Mn content increased, the material became increasingly fragile and the ribbons were formed in shorter pieces. By $x = 0.35$, millimeter flakes dominated production. Cu-K_α x-ray diffraction on an automated powder diffractometer was used to confirm the absence of crystalline contamination from all materials used in the measurements presented below. A bulk magnetic characterization (magnetization and ac susceptibility) was carried out on a commercial extraction magnetometer (Quantum Design PPMS). Data at 5 K in fields of up to 9 T (Fig. 1) show the rapid destruction of the magnetization as the Mn content is increased. Susceptibility measurements in a drive field of 1 mT at 377 Hz were used to follow the rapid decline in T_c that is also caused by the Mn doping. The divergence of the in-phase signal (χ') was used to identify T_c, while a clear peak in the out-of-phase (loss) response (χ'') provided an initial marker for

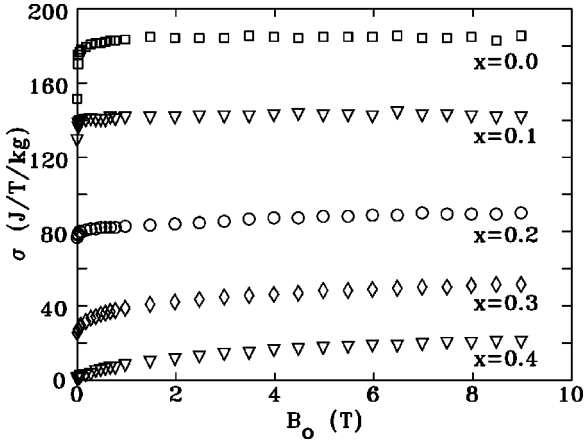

FIG. 1. Magnetization curves for several representative samples of a-$(Fe_{1-x}Mn_x)_{78}Si_8B_{14}$ measured at 5 K.

T_{xy}. Some typical data are shown in Fig. 2. Ordering temperatures for those alloys with T_c above 290 K ($x \leqslant 0.2$) were measured using a Perkin-Elmer thermogravimetric analyzer (TGA–7).

Mössbauer measurements were made on a constant acceleration spectrometer with a 1GBq ^{57}Co**Rh** source, calibrated using an α-Fe foil. Samples were mounted in a vibration-isolated closed-cycle refrigerator for spectra at temperatures down to 8 K. The spectra were fitted using Window's method[27] to obtain average hyperfine fields ($\langle B_{\rm hf} \rangle$) as a function of temperature. A linear correlation between $B_{\rm hf}$ and the isomer shift was included to account for the slight asymmetry in the spectra. Some typical spectra obtained at 8 K are shown in Fig. 3.

Zero-field μSR (ZF-μSR) measurements were made on the M20 beamline at TRIUMF. Sample temperature was controlled between 5 and 300 K in a conventional He-flow cryostat. Field zero was set to better than 1 μT using a three-axis flux-gate magnetometer. For $x \leqslant 0.15$, the μSR samples consisted of $\sim$15 layers of ribbons clamped between copper rings to give thicknesses of 170–200 mg cm^{-2} over a 16-mm-diameter active area. For $x \geqslant 0.20$, the material was crushed and approximately 1 g was mounted between a 99.99% pure silver foil and a 10-μm Kapton sheet within a

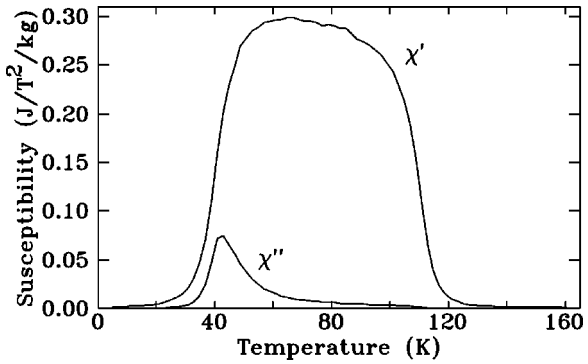

FIG. 2. ac susceptibility curves for a-$(Fe_{0.70}Mn_{0.30})_{78}Si_8B_{14}$ showing both the in-phase response (χ') used to obtain T_c and the peak in the out-of-phase signal (χ'') used to determine T_{xy}.

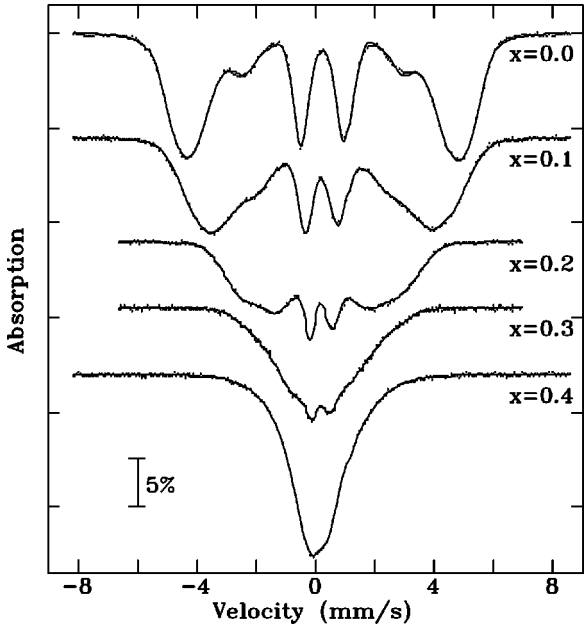

FIG. 3. ^{57}Fe Mössbauer spectra of several a-$(Fe_{1-x}Mn_x)_{78}Si_8B_{14}$ samples measured at 8 K. Solid lines are fits described in the text.

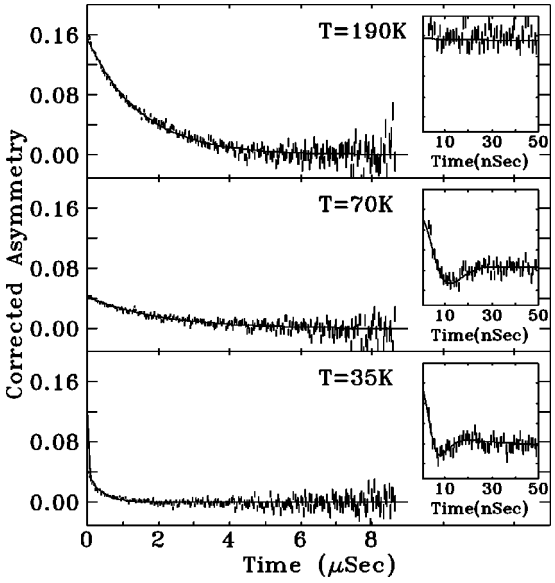

FIG. 4. ZF-μSR data for a-$(Fe_{0.725}Mn_{0.275})_{78}Si_8B_{14}$ measured above T_c (190 K) showing only exponential relaxation, in the ordered region above T_{xy} (70 K) showing both exponential and KT contributions, and just below T_{xy} (35 K) showing both contributions but a faster exponential relaxation due to the fluctuations associated with transverse spin freezing. Insets at each temperature show the early-time behavior. Solid lines are fits described in the text.

copper ring. A pure silver (99.99%) mask prevented stray muons from striking any of the mounting hardware. Essentially 100% spin polarized μ^+ were implanted with their moments directed in the backward direction (i.e., along $-z$). The subsequent decay e^+ is emitted preferentially along the moment direction. The time dependence of the μ^+ polarization is conventionally followed by plotting the asymmetry (A) between scintillation detectors placed in the forward (F) and backward (B) directions relative to the initial μ^+ flight direction $[A=(B-F)/(B+F)]$ as a function of time. Histograms containing $\sim 4\times 10^7$ events were acquired with a timing resolution of 0.781 ns. The relative efficiency of the forward and backward detectors was determined from late-time data near T_c, where the dynamic relaxation rate is the fastest, and the muons are fully depolarized quite early in the measuring window of ~ 10 μs. Under these conditions, any observed asymmetry between the forward and backward counters reflects unavoidable differences in the detector efficiencies (sensitivity, gain, energy thresholds, and geometrical factors are all significant contributors), which can therefore be measured and corrected for. The time dependence of this corrected asymmetry was then fitted using a conventional non-linear least-squares minimization routine.

Above T_c, fluctuations lead to an exponential dephasing of the muon polarization,

$$A_d = A_o \exp(-\lambda t), \tag{1}$$

where λ is an effective relaxation rate. A typical exponential decay above T_c is shown in Fig. 4 for $x=0.275$ at $T=190$ K. Below T_c, a static magnetic field will be present at the muon sites. However, the materials studied here are both structurally disordered (i.e., glassy) and magnetically disordered as a result of both random Mn substitution and also exchange frustration, therefore we expect a distribution of local fields to be present. In this case, the asymmetry will decay according to the Kubo-Toyabe (KT) form[28]

$$G_z(\Delta,t) = \frac{1}{3} + \frac{2}{3}[1-(\Delta t)^\alpha]\exp\left(-\frac{(\Delta t)^\alpha}{\alpha}\right), \tag{2}$$

with $\alpha=2$, so that Δ/γ_μ is the rms field. KT relaxation behavior is shown in the inset to the 35 K data in Fig. 4. The presence of a static component also accounts for the apparent loss of initial asymmetry on cooling through T_c (compare the main curves at 190 and 70 K in Fig. 4) as two-thirds of the muon polarization is lost in the first 30 ns. In cases where both static order and fluctuations are present (close to, but below, T_c, and also around T_{xy}), the asymmetry decays according to the product

$$A = A_d \times G_z, \tag{3}$$

and both a KT contribution at early times, and a slower exponential decay, are seen.

III. RESULTS AND DISCUSSION

Numerical simulations[5,19] indicate that the initial decline in the magnetization with Mn doping is due to the ordering of the moments antiparallel to the ferromagnetic iron matrix. Following the procedure used earlier,[17] the decline in the saturation magnetization in Fig. 5 can be analyzed to yield an average Mn moment of $3.1\pm 0.1\mu_B$, consistent with earlier work on this system.[17] Furthermore, the magnetization observed following field cooling to 5 K in 10 mT (Fig. 5) also shows a rapid decline with increasing x, going to zero just

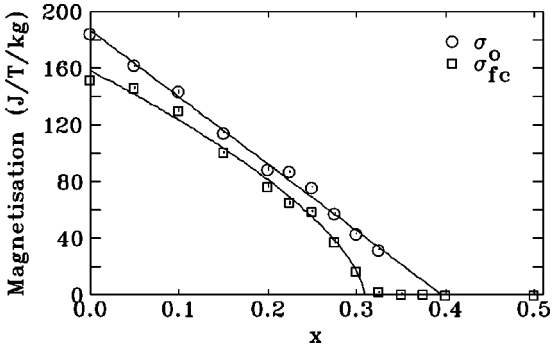

FIG. 5. Saturation magnetization derived from data in fields of 9 T (○) and field-cooled magnetization (□) obtained by cooling from above T_c to 5 K in a field of 10 mT. The collapse of σ_{fc} suggests that the critical composition for the loss of ferromagnetic order lies at $x=0.31$. Lines are guides to the eye.

above x = 0.30. A power law fits the observed dependence quite well, suggesting that the magnetization tracks an order parameter and that ferromagnetic order is lost entirely at a critical doping level (x_c) of 0.306 ± 0.006. Beyond this composition, the system is a spin glass.

The temperature dependence of the average hyperfine field $[\langle B_{\rm hf}\rangle(T)]$ shown in Fig. 6 exhibits a clear break in slope at T_{xy} for $x=0.25$, 0.275, and 0.30, outside this range T_{xy} is either absent ($x>x_c$ or $x<0.20$) or the contribution to $\langle B_{\rm hf}\rangle$ from the transverse spin components is too small to be reliably distinguished by this technique ($x=0.20$ and 0.225). This same behavior will be seen later in analyzing the static contribution to the μSR data. The observation of two clear transitions at $x=0.30$, and only one at $x=0.325$, places x_c between these two concentrations, in full agreement with the estimate derived from analysis of the field-cooled magnetization data. Fitting $\langle B_{\rm hf}\rangle(T)$ to a sum of two power-law functions allows us to extract estimates of T_c and T_{xy}. The

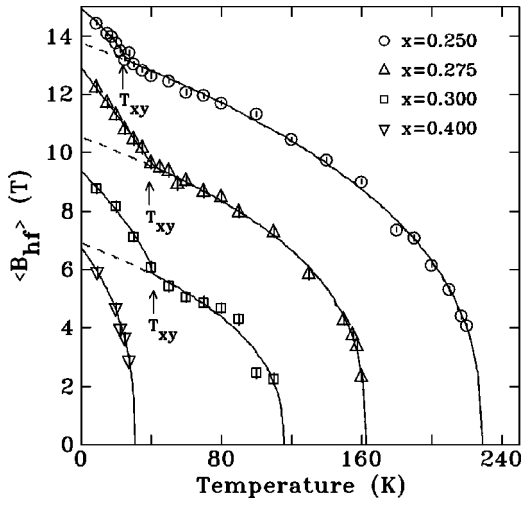

FIG. 6. Temperature dependence of the average hyperfine field $[\langle B_{\rm hf}\rangle(T)]$ for several a-$(Fe_{1-x}Mn_x)_{78}Si_8B_{14}$ samples around $x_c=0.31$. The break in slope is a clear marker of the increased static order at T_{xy}. Dotted lines show continuation of fits from above T_{xy}.

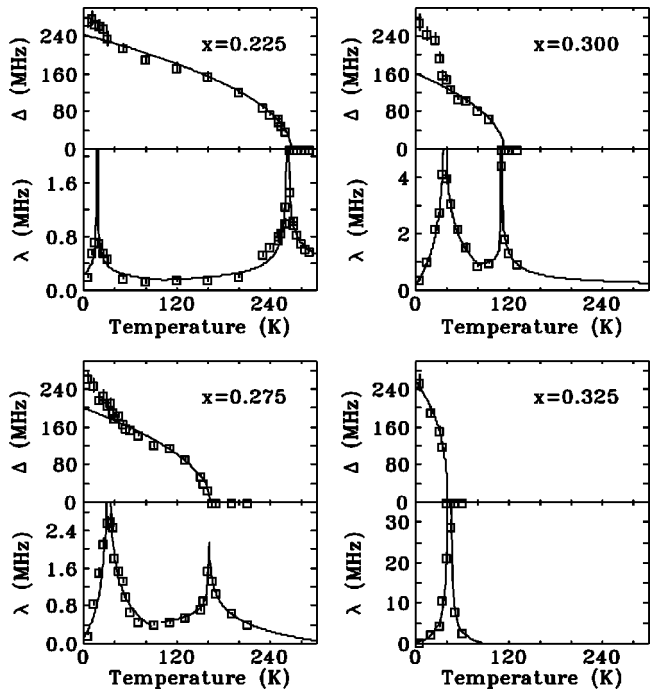

FIG. 7. Temperature dependence of the static (Δ) and dynamic (λ) signals from ZF-μSR for several a-$(Fe_{1-x}Mn_x)_{78}Si_8B_{14}$ alloys. In every case, the increase in static order (at T_c, T_{xy}, or T_{sg}) is associated with a peak in the fluctuation rate.

density of points used around T_{xy}, and the high statistical quality of the spectra (see Fig. 3) are both essential for this latter estimate to be stable. Remarkably, the values for T_{xy} derived from Mössbauer are in perfect agreement with those derived from χ'' above, suggesting that the dynamic loss feature seen in susceptibility is indeed closely associated with the onset of static transverse order. This agreement at three compositions does not support the earlier claim of distinct static (T_K) and dynamic (T_F) events below T_c.[20]

Fitting the μSR data using the functions described earlier yields the temperature dependences of the static relaxation rate (Δ), a measure of the static field seen by the muons, and the dynamic fluctuation rate (λ) which tracks the fluctuations in the field at the muon sites. These fits are summarized in Fig. 7 for four samples. The changeover from two transitions to one clearly occurs between $x=0.30$ and 0.325, again placing x_c in this range. Only a single transition is seen for the $x=0.350$ sample as it is beyond x_c and is therefore a spin glass. The four samples $0.225\leqslant x\leqslant 0.30$ each exhibit two distinct peaks in $\lambda(T)$. The higher temperature peak is associated with the onset of a non-zero static contribution and thus clearly corresponds to T_c, while the lower peak is aligned with the break in the slope of $\Delta(T)$ and therefore marks the freezing of the transverse spin components at T_{xy}. As the Mn content is reduced, the contribution of the transverse spin components to the total ordered moment declines, so that the increase in Δ below T_{xy} becomes difficult to localize reliably. Even with the high density of points apparent in Fig. 7, the error on T_{xy} at $x=0.225$ is about 16 K, however, the derived value is fully consistent with the two

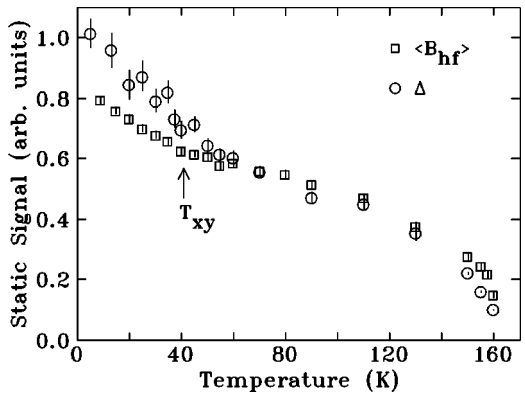

FIG. 8. Comparison of static order signals from Mössbauer spectroscopy ($\langle B_{hf}\rangle$) and ZF-μSR (Δ) for a-$(Fe_{0.725}Mn_{0.275})_{78}Si_8B_{14}$. The data have been normalized to agree above T_{xy} in order to compare the change and signal stability below T_{xy}.

dynamic determinations. At $x=0.20$, only the fluctuation peak at T_{xy} was detected.

Figure 8 shows a direct comparison between $\langle B_{hf}\rangle(T)$ and $\Delta(T)$ for a-$(Fe_{0.725}Mn_{0.275})_{78}Si_8B_{14}$, normalized to agree above T_{xy}. Both show a clear increase at T_{xy} confirming that they are each sensitive to the increased static order associated with the freezing of the transverse spin components. While there is a significant rise in $\langle B_{hf}\rangle(T)$ at T_{xy}, the change in the ZF-μSR data is much larger. This is to be expected as the Mössbauer measurement is dominated by the effects of the iron moment, while the muons will be affected equally by Mn and Fe moments. Indeed, in the a-$Fe_{90-x}Ru_xZr_{10}$ system,[8] where only iron moments are involved in the ordering, $\langle B_{hf}\rangle(T)$ and $\Delta(T)$ track together over the whole temperature range. However, the greater sensitivity of the ZF-μSR data comes with increased noise. As a time-domain technique, μSR is at its best in small fields. Large static fields drive the signal into very early times where resolution and timing issues eventually dominate the analysis. These effects are clearly illustrated by the scatter apparent below T_{xy}. By contrast, an energy-domain technique like Mössbauer spectroscopy works better in high fields and yields a more stable, albeit less marked, increase below T_{xy}.

The transition temperatures deduced from the ac-susceptibility data (χ' for T_c, χ'' for T_{xy}), $\langle B_{hf}\rangle(T)$ from Mössbauer spectroscopy, and both Δ and λ from the ZF-μSR data are summarized in the phase diagram shown in Fig. 9. Manganese doping has a severe effect on the magnetic ordering of this system, driving T_c down from 695 K at $x=0$ (inset to Fig. 9), to $\sim$40 K at $x_c=0.31$. A power law does not fit the composition dependence of T_c particularly well, and extrapolating T_c to zero yields a rather poor estimate for the critical composition of $x_c=0.33\pm0.02$. This failure is not unexpected, as the FM-SG boundary is *not* marked by $T_c\rightarrow 0$, but rather by $T_c\rightarrow T_{xy}$. Indeed, a power-law fit to $1\text{-}T_{xy}/T_c$ is far superior, and yields $x_c=0.309\pm0.004$, in perfect agreement with $x_c=0.306\pm0.006$ derived earlier from field-cooled magnetization data.

The excellent agreement between T_c values derived from

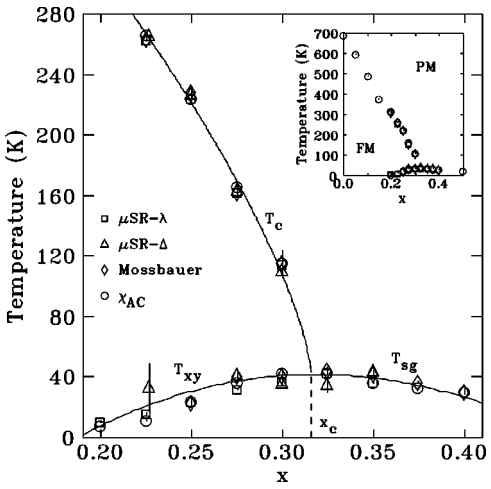

FIG. 9. Magnetic phase diagram for a-$(Fe_{1-x}Mn_x)_{78}Si_8B_{14}$ derived from ac-susceptibility data (χ' for T_c, χ'' for T_{xy}), $\langle B_{hf}\rangle\times(T)$ from Mössbauer spectroscopy, and both Δ and λ from the ZF-μSR. Three transitions can be identified: ferromagnetic ordering at T_c, transverse spin freezing at T_{xy}, and spin glass ordering only for $x>x_c$ at T_{sg}. Note the perfect agreement between independent determinations of T_{xy}. The inset shows data for the whole composition range studied.

χ', Mössbauer spectroscopy, and ZF-μSR, coupled with consistent T_{sg} values obtained above x_c, provides strong evidence that the analysis and transition assignments are correct and self-consistent. However, it is the behavior at T_{xy} that is the primary focus of this work. Only for $x\geqslant 0.2$ do we see a second transition below T_c, a result that is in full accord with numerical simulations.[5,19] There is excellent agreement between T_{xy} values derived from the various techniques. For $x=0.275$ and 0.300, we have four independent determinations of T_{xy} that agree to better than 5 K. The static, dynamic, and loss signatures of T_{xy} are in perfect agreement, with no systematic bias apparent in any of the measurements. While at $x=0.250$, static data from Mössbauer, and dynamics from both $\lambda(T)$ and χ'' are in complete agreement. By $x=0.225$, the change in the static order at T_{xy} is too small for its onset to be reliably determined from $\langle B_{hf}\rangle(T)$ and the estimate from $\Delta(T)$ exhibits a substantial ($\sim$50%) uncertainty. However the ZF-μSR fluctuation peak, and the maximum in the χ'' loss signal are still clear and coincident. As was found in our earlier work on bond-frustrated alloys,[7,8,25,26] all observed signatures of T_{xy} line up perfectly.

It is important to emphasize that the techniques that have been used to determine T_{xy} with such good agreement probe a very wide range of frequencies: ZF-μSR–Δ ($\sim 10^8$ Hz), $\langle B_{hf}\rangle$-Mössbauer ($\sim 10^7$ Hz), ZF-μSR-λ ($\sim 10^6$ Hz), and χ'' ($\sim 10^2$ Hz), yet they yield T_{xy} values that agree within a few K for five samples that exhibit transverse spin freezing transitions at temperatures that change by more than a factor of three. Furthermore, there is no systematic frequency related trend in the T_{xy} values for a given sample. The scatter is random. A separation of T_{xy} into distinct static (T_K) and dynamic (T_F) events can therefore be ruled out. There is no

evidence in our data to support the existence of a third transition below T_{xy}.

IV. CONCLUSIONS

Zero-field μSR, Mössbauer spectroscopy and ac-susceptibility provide clear evidence of a single transverse spin freezing transition in the site-frustrated a-$(Fe_{1-x}Mn_x)_{78}Si_8B_{14}$ alloy system. This behavior matches that seen earlier in bond-frustrated alloys,[7,8,25,26] and our phase diagram for a-$(Fe_{1-x}Mn_x)_{78}Si_8B_{14}$ is fully consistent with the results of numerical simulations on site-frustrated Heisenberg spin systems.[5,19] We find no evidence of the previously reported mismatch in transition temperatures derived from dynamic and static signatures,[20] nor do we see any indication of a third transition below T_c and T_{xy}.

ACKNOWLEDGMENTS

The authors would like to acknowledge assistance from the TRIUMF muon group during the acquisition of this data. D.H.R. is grateful for the hospitality of the School of Physics at The University of New South Wales, Australia where much of the initial work was carried out. This work was supported by grants from: the Natural Sciences and Engineering Research Council of Canada, Fonds pour la formation de chercheurs et l'aide à la recherche, Québec, and the Australian Research Council.

[1] D.H. Ryan in *Recent Progress in Random Magnets*, edited by D.H. Ryan (World Scientific, Singapore, 1992), pp. 1–40.
[2] H. Ren and D.H. Ryan, Phys. Rev. B **51**, 15 885 (1995).
[3] J.R. Thomson, Hong Guo, D.H. Ryan, M.J. Zuckermann, and M. Grant, Phys. Rev. B **45**, 3129 (1992).
[4] M. Gabay and G. Toulouse, Phys. Rev. Lett. **47**, 201 (1981).
[5] Morten Nielsen, D.H. Ryan, Hong Guo, and Martin Zuckermann, Phys. Rev. B **53**, 343 (1996).
[6] D.H. Ryan, Zin Tun, and J.M. Cadogan, J. Magn. Magn. Mater. **177-81**, 57 (1998).
[7] D.H. Ryan, J.M. Cadogan, and J. van Lierop, Phys. Rev. B **61**, 6816 (2000).
[8] D.H. Ryan, J.M. Cadogan, and J. van Lierop, Phys. Rev. B **62**, 8638 (2000).
[9] J. van Lierop and D.H. Ryan, Phys. Rev. Lett. **86**, 4390 (2001).
[10] C.L. Chien, J.H. Hsu, P.J. Viccaro, B.D. Dunlap, G.K. Shenoy, and H.S. Chen, J. Appl. Phys. **52**, 1750 (1981).
[11] H. Keller, K.V. Rao, P.G. Debrunner, and H.S. Chen, J. Appl. Phys. **52**, 1753 (1981).
[12] I. Mirebeau, G. Jehanno, I.A. Campbell, F. Hippert, B. Hennion, and M. Hennion, J. Magn. Magn. Mater. **54-57**, 99 (1986).
[13] J.A. Geohegan and S.M. Bhagat, J. Magn. Magn. Mater. **25**, 17 (1981).
[14] G. Aeppli, S.M. Shapiro, H. Maletta, R.J. Birgeneau, and H.S. Chen, J. Appl. Phys. **55**, 1628 (1984).
[15] K. Heinemann, C. Michaelsen, M. Fieber, and K. Baerner, J. Magn. Magn. Mater. **82**, 204 (1989).
[16] T. Miyazaki, I. Okamoto, Y. Ando, and M. Takahashi, J. Phys. F: Met. Phys. **18**, 1601 (1988).
[17] A. Kuprin, D. Wiarda, and D.H. Ryan, Phys. Rev. B **61**, 1267 (2000).
[18] T. Ersez, S.J. Kennedy, and T.J. Hicks, J. Phys.: Condens. Matter **7**, 8423 (1995).
[19] A. Beath and D.H. Ryan, J. Appl. Phys. (to be published 15 May 2003).
[20] I. Mirebeau, M. Hennion, M.J.P. Gingras, A. Keren, K. Kojima, M. Larkin, G.M. Luke, B. Nachumi, W.D. Wu, Y.J. Uemura, I.A. Campbell, and G.G. Morris, Hyperfine Interact. **104**, 343 (1997).
[21] H. Keller, K.V. Rao, P.G. Debrunner, and H.S. Chen, J. Appl. Phys. **52**, 1753 (1981); I. Mirebeau, G. Jehano, M. Hennion, and I.A. Campbell, J. Magn. Magn. Mater. **54**, 99 (1986).
[22] M. Hennion, I. Mirebeau, B. Hennion, S. Lequien, and F. Hippert, Europhys. Lett. **2**, 393 (1986); I. Mirebeau, M. Hennion, S. Lequien, and F. Hippert, J. Appl. Phys. **63**, 4077 (1988).
[23] B. Hennion, M. Hennion, I. Mirebeau, and F. Hippert, Physica B **136**, 49 (1986); M. Hennion, B. Hennion, I. Mirebeau, S. Lequien, and F. Hippert, J. Appl. Phys. **63**, 4071 (1988).
[24] I. Mirebeau, S. Itoh, S. Mitsuda, T. Watanabe, Y. Endoh, M. Hennion, and R. Papoular, Phys. Rev. B **41**, 11 405 (1990).
[25] D.H. Ryan, J.M. Cadogan, and J. van Lierop, J. Appl. Phys. **87**, 6525 (2000).
[26] D.H. Ryan, J. van Lierop, M.E. Pumarol, M. Roseman, and J.M. Cadogan, J. Appl. Phys. **89**, 7039 (2001).
[27] B. Window, J. Phys. E **4**, 401 (1971).
[28] R. Kubo, Hyperfine Interact. **8**, 731 (1981); R. Kubo and T. Toyabe, in *Magnetic Resonance and Relaxation*, edited by R. Blinc (North-Holland, Amsterdam, 1967), p. 810.